This article has been accepted for publication in a future issue of this journal, but has not been fully edited. Content may change prior to final publication. Citation information: DOI 10.1109/LAWP.2015.2404875, IEEE Antennas and Wireless Propagation Letters

A Palm Tree Antipodal Vivaldi Antenna with Exponential Slot Edge for Improved Radiation Pattern

Alexandre M. De Oliveira, *Student Member, IEEE*, Marcelo B. Perotoni, Sergio T. Kofuji, and João F. Justo

***Abstract*— This letter presents an Exponential Slot Edge Antipodal Vivaldi Antenna (ESE-AVA), with improved radiative features as compared to the conventional Antipodal Vivaldi Antenna (AVA) design. It extends the low-end bandwidth limitation, mitigates the side and back lobe levels, corrects squint effect, and increases its main lobe gain. In order to confirm those features, a comparative study among the ESE-AVA, the low directivity conventional AVA and two popular modifications, regular slot edge (RSE) and the tapered slot edge (TSE) AVA is performed. A comparison between AVA and the proposed ESE-AVA at 6 GHz shows an improved gain of 8.3 dB, -15.5 dB of Side Lobe Level (SLL), and 0 degrees of main lobe squint (MLS), in contrast with 5 dB of gain, -5 dB of SLL, and 5 degrees of MLS in the conventional AVA. By comparing the ESE-AVA with RSE-AVA and TSE-AVA, it was observed that its notches in exponential shape, similar to open the main radiator, besides mitigating the SLL also directs the E-fields distributions towards the main lobe. It reflects into a main lobe gain improvement.**

***Index Terms*—ultra-wideband, Antipodal Vivaldi Antenna, Directivity Improvement.**

I. Introduction

THE Vivaldi antenna was originally designed more than 30 years ago in a coplanar shape [1], and was later developed in an antipodal shape [2]. It is an ultra-wideband device which has drawn great attention from researchers, and has been considered for applications in essentially all microwave systems, such as in imaging medicine [3], radar systems [4, 5], astronomy [6], vehicular communication [7], and through-wall localization [8].

The AVA is suitable for applications in compact systems, either in single form or in an array, due to its lightweight and small dimensions. It is a directive wideband antenna with high efficiency and gain, which can be integrated directly into a circuit board [8-11]. Despite such features, the Vivaldi antenna still has its shortcomings. The original design, especially its side edges, increases the SLL coming from edge currents, which compromises antenna directivity, in addition to a squint on its radiation pattern, which compromises the directional control of the main lobe (ML). Over the last few years, several antenna designs have been proposed, in order to mitigate this problem, using directors in many forms, such as dielectrics [3, 12, 13] and metamaterials [14], which compromises its main constructive qualities, increasing the final antenna dimensions and making its design complex.

In order to reduce the SLL of an AVA, a tapered slot edge (TSE) has been recently used [12, 15, 16], which also improves directivity, without increasing the volume of the antenna, but no additional gain for the antenna was reported. The TSE design inhibited edge currents, which would promote the emergence of side lobes, acting as a resonator. Therefore, by removing edge currents, there is a relevant attenuation on the SLL of the AVA [7, 12, 15-17].

Here, it is presented a new design for the Vivaldi Antenna, featuring a slot edge with exponential opening similar to the opening of the main radiator, called Exponential Slot Edge (ESE). Comparing with a conventional AVA, the new antenna simultaneously reduces the SLL, corrects squint effect and increases the gain of the ML. As a result, it provides improvements on the radiation characteristics, in terms of directivity and gain, with a simple design and without increasing the antenna dimension.

This letter is organized as follows: Section II presents the antenna design, Section III presents the numerical analysis, experiments and results. Finally, Section IV presents concluding remarks.

II. Antenna Design

Fig. 1(a) presents a traditional AVA, while Fig. 1(b) presents the proposed ESE-AVA (in metal layers only), here named Palm Tree antenna. This new design tries to decrease (in controlled manner) surface current intensities on the antenna edges, consequently decreasing the AVA SLL, expanding the low frequency limit, and increasing the ML gain.

The improvements do not change the antenna dimensions, when comparing AVA and ESE-AVA, which corresponds to an occupied area of 36.3 x 59.81 mm², with the same 0.64 mm substrate thickness. This antenna is considerably smaller than in other investigations [7, 11, 14, 15]. Additional miniaturization is possible by using substrates with high dielectric constant, such as LTCC or Alumina.

Manuscript received November 18, 2014; revised January 16, 2015; accepted February 14, 2015. First published Mmm dd, yyyy; current version published Mmm dd, yyyy.

A. M. De Oliveira, S. T. Kofuji, and J. F. Justo are with the Department of Electronic Systems Engineering in the Polytechnic School of the University of São Paulo, CEP 05508-900, São Paulo, SP, Brazil. (a.m.deoliveira@ieee.org).

M. B. Perotoni is with ABC Federal University, CEP 09210-180, Santo André, SP, Brazil. (marcelo.perotoni@ufabc.edu.br)

Color version of one or more of the figures in this letter are available online at http://ieeexplore.ieee.org.

Digital Object Identifier 10.1109/LAWP.2014.XXXXXX

This article has been accepted for publication in a future issue of this journal, but has not been fully edited. Content may change prior to final publication. Citation information: DOI 10.1109/LAWP.2015.2404875, IEEE Antennas and Wireless Propagation Letters

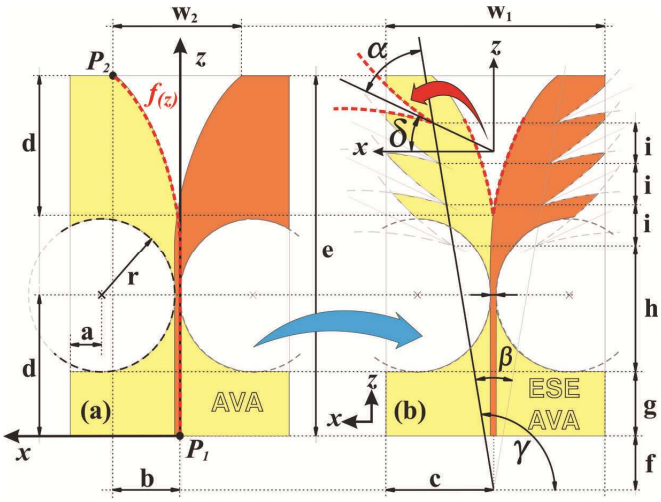

Fig. 1. Design and antenna parameters in xz-plane: (a) reference AVA. (b) proposed ESE-AVA.

The antenna is formed by a microstrip transition line (MTL), a main exponential slot radiator (MESR), and ESEs. The MTL has a length of 23.02 mm and a width of 1 mm on a Rogers RO3206 substrate with dielectric constant of 6.15 and tangential loss of 0.0027, in order match with 50 Ω of SMA connector. The MESR is designed, according to Ref. [18], by the exponential curve ***f (z)***, given by equations (1), (2) and (3), defined by the opening rate (R=0.105) and the points ***P₁(z₁,x₁)*** and ***P₂(z₂,x₂)***, shown in Fig. 1.

$$f(z) = c_1 e^{Rz} + c_2 \tag{1}$$

where

$$c_1 = \frac{x_2 - x_1}{e^{Rz_2} - e^{Rz_1}} \tag{2}$$

and

$$c_2 = \frac{x_2 e^{Rz_2} - x_1 e^{Rz_1}}{e^{Rz_2} - e^{Rz_1}} \tag{3}$$

Fig. 2 shows the palm tree antenna, the picture on the left shows a top view, while the one on the right shows a bottom view.

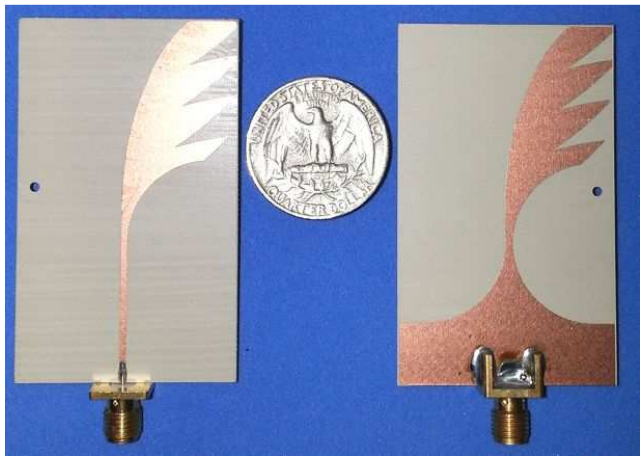

Fig. 2. Fabricated ESE-AVA photograph, top view on the left and bottom view on the right.

Table I presents the antenna dimensional parameters. The ESEs, that have the same exponential opening of the MESR, are added on the side of the antenna and are rotated slightly (δ=25º) with respect to the perpendicular antenna propagation direction, in order to promote the surface currents control at edges, simultaneously decreasing the lower limit of the bandwidth and increasing the gain of the ML.

TABLE I - PARAMETERS OF THE AVA AND ESE-AVA ARCHITECTURES.

Dimension parameters						Angles	
a	4.03	e	59.81	i	6.87	α	55º
b	11.17	f	5.91	r	13.12	β	20º
c	18.15	g	9.97	w_1	36.30	γ	100º
d	23.02	h	21.59	w_2	21.35	δ	25º

The parameters a, b, c, d, e, g, r, w_1, and w_2 are identical for AVA, RSE-AVA, TSE-AVA and ESE-AVA architectures shown in this letter. Dimensions are given in mm.

III. 3D NUMERICAL AND EXPERIMENTAL RESULTS

The design of the ESE-AVA was performed in two steps [19]. The first one is an optimization of the antenna characteristics by 3D numerical simulations, while the second one is associated to experimental measurements on a prototype antenna with optimized parameters.

Numerical analysis was performed using the software CST Microwave Studio. The AVA and its volumetric surroundings are represented by a 3D mesh matrix of 212 x 53 x 335 cells respectively in ***x***, ***y***, and ***z*** directions, which represent more than 3.7 million of cells. Additional open space of 20 mm was considered on each side of the antenna (***x*** direction), as well as 15 and 40 mm respectively in its front and back (***z*** direction).

The simulations were performed with the CST Transient Solver, and some parameters were adjusted for the modeling of the matrix, such as a density of 15 cells per wavelength at 8 GHz with a bandwidth between 0 to 16 GHz. The parameter PEC/lossy metal edges factor was adjusted to 6. The other parameters were left as default.

In order to mimic a real system, the SMA connector, shown in Fig. 3(a), was modeled and integrated in the AVAs models, based on a Multicomp SMA connector, specific for the 0.64 mm substrate thickness, used in the manufactured antenna, shown in Fig. 3(b).

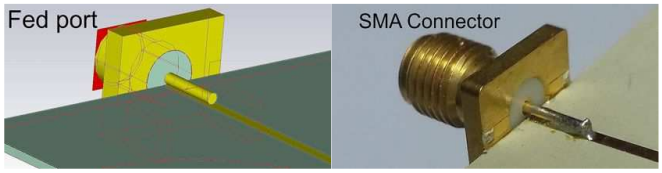

(a) **(b)**

Fig. 3. SMA connector: (a) in numerical model and (b) at ESE-AVA.

The experimental measurements were performed in two steps. The S parameters were measured, outside the chamber, using a HP 8722D Network Analyzer, while the measurements of the radiation pattern, inside the chamber, were performed using the following setup: the transmitter system (fixed) is formed by an HP 8350B Sweep Oscillator and an HP 8359A RF Plug-in 2 to 8.4 GHz. The receiver system is formed by the antenna under test and the HP436A Power Meter, equipped with HP8470D Power Sensor – the system turns around mechanically.

Fig. 4 presents the measured and simulated reflection coefficient (S_{11}) of the AVA and ESE-AVA. As reported by

This article has been accepted for publication in a future issue of this journal, but has not been fully edited. Content may change prior to final publication. Citation information: DOI 10.1109/LAWP.2015.2404875, IEEE Antennas and Wireless Propagation Letters

Refs. [12, 15, 17], the lower limit frequency is reduced from 5.08 to 4.73 GHz. The results are in good agreement with the ones obtained by numerical simulations, observing the ESE-AVA compatibility with ultra-wideband (UWB) applications, especially from 5.6 GHz to more than to 11 GHz.

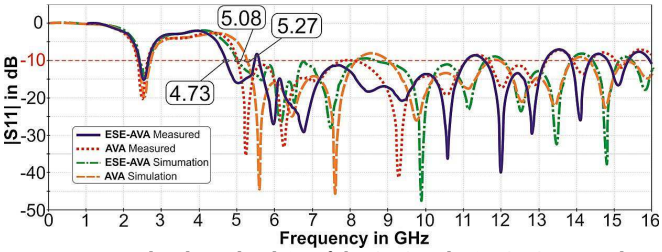

Fig. 4. Measured and simulated S_{11} of the AVA and ESE-AVA. Lower limit frequency reduction of ESE-AVA in details.

In order to perform a comparison among several antenna designs, which have been proposed recently, modifications were made to the reference AVA, shown in Fig. 5(a). Two types of slot resonator edges were considered: the regular edge slot (RSE), shown in Fig. 5(b), and the tapered slot edge (TSE), shown in Fig. 5(c). The WR1 width is equal to 9.3 mm, while the WR2 width is equal to 12.3 mm.

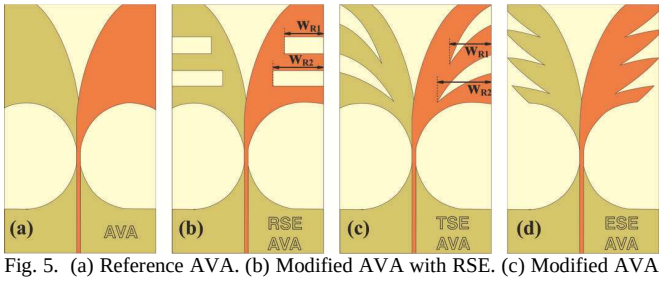

Fig. 5. (a) Reference AVA. (b) Modified AVA with RSE. (c) Modified AVA with TSE. (d) Proposed AVA with ESE.

Fig. 6 shows the S_{11} parameter of the AVA, ESE-AVA, RSE-AVA, and TSE-AVA systems.

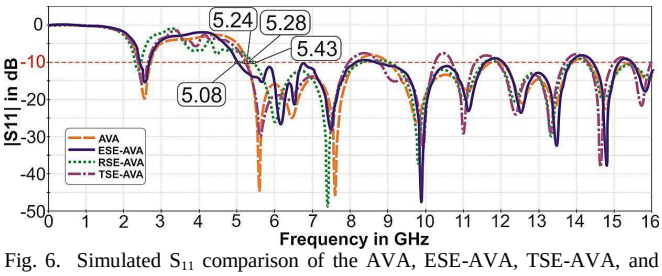

Fig. 6. Simulated S_{11} comparison of the AVA, ESE-AVA, TSE-AVA, and RSE-AVA. Lower limit frequency reduction of ESE-AVA in details.

In the simulations, the lower frequency limit of AVA is 5.28 GHz, while of ESE-AVA is 5.08 GHz, and of TSE-AVA is 5.24 GHz. The RSE-AVA presented a worst lower limit of 5.43 GHz.

Fig. 7 shows the simulated gains for the conventional AVA and three modifications (ESE-AVA, RSE-AVA and TSE-AVA). The gain improvement promoted by the ESE at 6 GHz is greater than 3 dB, and remains around 8 dB up to 14 GHz. This almost constant gain, which is not observed in any other AVA, is an ideal feature for UWB radar applications. This is due to the relationship of the respective wavelengths and the distances between the notched ESEs, on the edges of antenna.

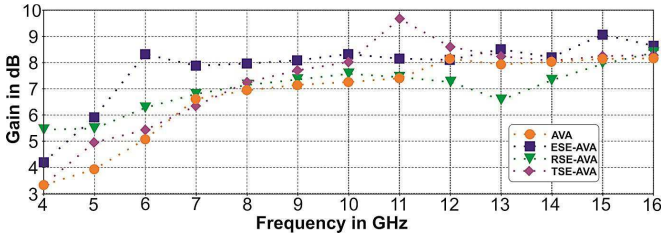

Fig. 7. Simulated gains of AVA, ESE-AVA, RSE-AVA, and TSE-AVA.

Fig. 8 provides additional elements to confirm that the proposed ESE promotes improvement on directivity and gain with respect to the conventional AVA, RSE-AVA and TSE-AVA. The ESEs that are notched with the same exponential opening shape as of the main radiator promote optimal conditions to avoid the trapping of E and H fields, as occurs in conventional slot edges, such as observed in Refs. [12, 15-17].

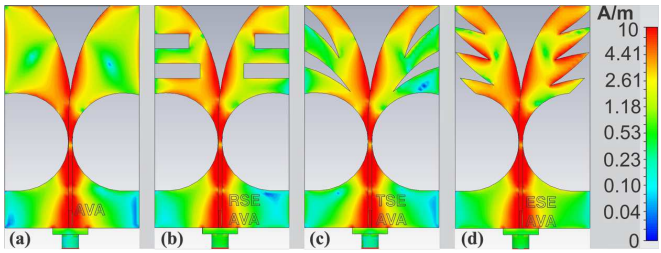

Fig. 8. Surface current of (a) AVA, (b) RSE-AVA, (c) TSE-AVA, and (d) ESE-AVA at 6 GHz.

The improvement on the characteristic radiation of an ESE-AVA is due to the control of current distribution near the lateral antenna edges. In the AVA, in Fig. 8(a), the secondary current distributions are concentrated at the side edges, leading to a high radiation SL of the order of 0 dB at 6 GHz. In both RSE-AVA, in Fig. 8(b), and TSE-AVA, in Fig. 8(c), there is confinement of E and H fields in the resonator path, since the notches trap polarized surface currents. Hence, although the radiation generated by them considerably reduces the SLL, there is no significant improvement on ML. In the ESE-AVA, in Fig. 8(d), there is an interesting effect, controlling the current distribution similarly to what happens in MESR, which for some moments enhances the main lobe radiation (in contrast to trapping in RSE and TSE), besides promoting the reduction of SLL.

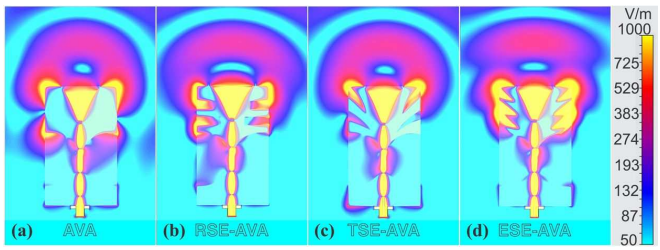

Fig. 9. E-field distribution in xz-plane at 6 GHz for (a) AVA, (b) RSE-AVA, (c) TSE-AVA, and (d) ESE-AVA at 6 GHz.

As a result of surface current distribution on the antenna, an E-field radiation pattern emerges, which is illustrated in Fig. 9. The E-field distribution in different directions is promoted in the AVA, in Fig. 9(a). Both RSE-AVA, in Fig. 9(b), and TSE-AVA, in Fig. 9(c), trapped E-fields inside the slot edges, which reduces the lateral E-field distribution considerably, but the front-distribution (endfire) remains

This article has been accepted for publication in a future issue of this journal, but has not been fully edited. Content may change prior to final publication. Citation information: DOI 10.1109/LAWP.2015.2404875, IEEE Antennas and Wireless Propagation Letters

almost unchanged when compared to AVA.

In the ESE-AVA, the ESEs format is similar to the MESR, providing a controlled and directional radiation of the E-fields, which is combined (added) with the front E-field radiation (endfire), as illustrated in Fig. 9(d). In addition to reduce SLL, the ESE-AVA provides higher gain. Fig. 10(a) shows that at 6 GHz the gain goes from 5 dB in AVA to 8.3 dB in ESE-AVA.

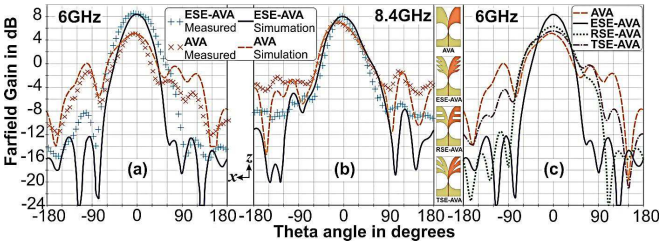

Fig. 10. Measured and simulated radiation pattern at (a) 6 and (b) 8.4GHz of the AVA and ESE-AVA. (c) Simulated radiation pattern at 6GHz of the AVA (dashed-line), ESE-AVA (solid-line), RSE-AVA (doted-line), and TSE-AVA (dotdashed-line).

Figs. 10(a) and (b) display the radiation patterns for co-polarization at 6 and 8.4 GHz, respectively. There is a good agreement between simulated and measured values, confirming that the ESE reduces SLL and increases the ML gain. At 6 GHz, the ML gain is 3.3 dB higher in ESE-AVA than in AVA. Another interesting aspect is the effect of the squint correction. In the reference-AVA it was 5 degrees, and in the ESE-AVA it is 0 degrees. This suggests that ESE-AVA is suitable for Phased and Timed-array applications [5]. Fig. 10(c) shows that although all three modified antennas (RSE-AVA, TSE-AVA and ESE-AVA) decrease the SLL, only ESE-AVA increases the ML gain.

Table II compares AVA with the ESE-AVA.

TABLE II - COMPARISON BETWEEN THE AVA AND THE ESE-AVA.

Freq.	Gain in dB at			SLL in dB at			Squint	Lower freq.	
in GHz.	6	9	12	6	9	12	at 6	Simul.	Meas.
AVA	5.0	7.1	8.1	-5.0	-10.3	-7.0	5º	5.28	5.08
ESE-AVA	8.3	8.1	8.1	-20.5	-11.6	-7.1	0º	5.08	4.73

The simulated group delay time result shows an average value of 0.31 ns with variation of the +/-2.5 ns within the bandwidth range (5 to 16GHz).

IV. CONCLUSIONS

This letter presents a new AVA, called Palm Tree antenna. It promotes the control of surface currents along the antenna edges, thereby enhancing the MESR. As a result, there is a major reduction in SLL and an increase in the main lobe gain, improving the endfire radiation characteristics of the antenna. The simulated and measured results indicated that at a frequency of 6 GHz, there was a better performance of ESE-AVA compared to traditional AVA, because the distance between the ESEs are related to the wavelengths, and for that frequency there was an improvement in gain of 3.3 dB, and a decrease SLL of -15.5 dB compared to the conventional AVA. Over the remaining frequencies, the ESE technique provides an almost constant gain, up to 14 GHz, and present values of S_{11} smaller than -10 dB between 5.6 and 11 GHz. Those features highlight its characteristics for UWB applications. Finally, the new design also led to a squint correction from 5 to 0 degrees. The addition of these ESEs promoted an important improvement in antenna directivity.

ACKNOWLEDGMENTS

The authors acknowledge Prof. Fátima Salete Correra, technicians Jair Pereira de Souza and Wesley Becari for helping on measurements, and Rogers Co. for supplying the laminates.

REFERENCES

[1] P. J. Gibson, "The Vivaldi Aerial," in Proc. *IEEE 9th Eur. Microw. Conf.* pp. 101-105, 1979.

[2] E. Gazit, "Improved design of the Vivaldi antenna," *IEE Proc. Microw. Anten. Propag.* vol. 135, no. 2, pp. 89-92, Apr. 1988.

[3] J. Bourqui, M. Okoniewski, and E. C. Fear, "Balanced antipodal Vivaldi antenna with dielectric director for near-field microwave imaging," *IEEE Trans. Anten. Propag*., vol. 58, no. 7, pp. 2318-2326, Jul. 2010.

[4] X. Zhuge and A. G. Yarovoy, "A sparse aperture MIMO-SAR-based UWB imaging system for concealed weapon detection," *IEEE Trans. Geosc. Rem. Sens.*, vol. 49, no. 1, pp. 509-518, Jan. 2011.

[5] J. D. S. Langley, P. S. Hall, and P. Newham, "Balanced antipodal Vivaldi antenna for wide bandwidth phased arrays," *IEE Proc. Microw. Anten. Propag.*, vol. 143, no. 2, pp. 97-102, Apr. 1996.

[6] E. W. Reid, L. O. Balbuena, A. Ghadiri, and K. Moez, "A 324-element Vivaldi antenna array for radio astronomy instrumentation," *IEEE Trans. Instrum. Meas.*, vol. 61, no. 1, pp. 241-250, Jan. 2012.

[7] S. H. He, W. Shang, C. Fan, Z. C. Mo, F. H. Yang, and J. H. Chen, "An improved Vivaldi antenna for vehicular wireless communication systems", *IEEE Anten. Wirel. Propag. Lett.*, vol. 13, pp. 1505-1508, Aug. 2014.

[8] Y. Yang, Y. Wang, and A. E. Fathy, "Design of compact Vivaldi antenna arrays for UWB see through wall applications," *Prog. Electromag. Resea*., vol. 82, pp. 401-418, 2008.

[9] A. Z. Hood, T. Karacolak, and E. Topsakal, "A small antipodal Vivaldi antenna for ultrawide-band applications," *IEEE Anten. Wirel. Propag. Lett.*, vol. 7, pp. 656-660, Mar. 2008.

[10] S. Chamaani, S. Mirtaheri, and M. S. Abrishamian, "Improvement of time and frequency domain performance of antipodal Vivaldi antenna using multi-objective particle swarm optimization," *IEEE Trans. Anten. Propag.*, vol. 59, no. 5, pp. 1738-1742,May 2011.

[11] Y. W. Wang, G. M. Wang, and B. F. Zong, "Directivity improvement of Vivaldi antenna using double-slot structure," *IEEE Anten. Wirel. Propag. Lett*., vol. 12, pp. 1380-1383, Oct. 2013.

[12] L. Juan, F. Guang, Y. Lin, and F. Demin, "A modified balanced antipodal Vivaldi antenna with improved radiation characteristics," *Microw. Optic. Thec. Lett*., vol. 55, no. 6, pp. 1321-1325, Jun. 2013.

[13] R. Kazemi, A. E. Fathy, and R. A. Sadeghzadeh, "Dielectric rod antenna array with substrate integrated waveguide planar feed network for wideband applications," *IEEE Trans. Anten. Propag*., vol. 60, no. 3, pp. 1312-1319, Mar. 2012.

[14] B. Zhou, H. Li, X. Y. Zou, and T. J. Cui, "Broadband and high-gain planar Vivaldi antennas based on inhomogeneous anisotropic zero-index metamaterials," *Prog. Electromag. Resea*., vol. 120, pp. 235-247, 2011.

[15] P. Fei, Y. C. Jiao, W. Hu, and F. S. Zhang, "A miniaturized antipodal Vivaldi antenna with improved radiation characteristics," *IEEE Anten. Wirel. Propag. Lett.*, vol. 10, pp. 127-130, Feb. 2011.

[16] F. Taringou, D. Dousset, J. Bornemann, and K. Wu, "Broadband CPW feed for millimeter-wave SIW-based antipodal linearly tapered slot antenna," *IEEE Trans. Anten. Propag*., vol. 61, no. 4, pp. 1756-1762, Apr. 2013.

[17] J. Bai, S. Shi, and D. W. Prather, "Modified compact antipodal vivaldi antenna for 4-50-GHz UWB application," *IEEE Trans. Microw. Theory Techn.*, vol. 59, no. 4, pp. 1051-1057, Apr. 2011.

[18] J. Shin and D. H. Schaubert, "A parameter study of stripline-fed Vivaldi notch-antenna arrays," *IEEE Trans. Anten. Propag*., vol. 47, no. 5, pp. 879-886, May. 1999.

[19] T. Thomas, M. Timm, and I. Munteanu, "A practical guide to 3-D simulation," *IEEE Microw. Magaz*., vol. 9, no. 6, pp. 62-75, Dec 2008.